HHS Public Access

Author manuscript

Nano Lett. Author manuscript; available in PMC 2020 October 09.

Published in final edited form as:

Nano Lett. 2019 October 09; 19(10): 7334–7341. doi:10.1021/acs.nanolett.9b02958.

Aptamer-Conjugated Framework Nucleic Acids for the Repair of Cerebral Ischemia-Reperfusion Injury

Shiyong Li[†,‡], **Dawei Jiang**[*,‡], **Zachary T. Rosenkrans**[‡,§], **Todd E. Barnhart**[‡], **Emily B. Ehlerding**[‡], **Dalong Ni**[‡], **Jonathan W. Engle**[‡], **Weibo Cai**[*,‡,§]

[†]Department of Rehabilitation, Second Affiliated Hospital of Nanchang University, Jiangxi 330006, China

[‡]Departments of Radiology and Medical Physics, University of Wisconsin-Madison, Madison, Wisconsin 53705, United States

[§]Department of Pharmaceutical Sciences, University of Wisconsin-Madison, Madison, Wisconsin 53705, United States

Abstract

Effective therapy for protecting dying neurons against cerebral ischemia-reperfusion injury (IRI) represents a substantial challenge in the treatment of ischemic strokes. Oxidative stress coupled with excessive inflammation is the main culprit for brain IRI that results in neuronal damage and disability. Specifically, complement component 5a (C5a) exacerbates the vicious cycle between oxidative stress and inflammatory responses. Herein, we propose that a framework nucleic acid (FNA) conjugated with anti-C5a aptamers (aC5a) can selectively reduce C5a-mediated neurotoxicity and effectively alleviate oxidative stress in the brain. Intrathecal injection of the aC5a-conjugated FNA (aC5a-FNA) was applied for the treatment of rats with ischemic strokes. Positron emission tomography (PET) imaging was performed to investigate the accumulation of aC5a-FNA in the penumbra and its therapeutic efficacy. Results demonstrated that aC5a-FNA could rapidly penetrate different brain regions after brain IRI. Furthermore, aC5a-FNA effectively protected neurons from brain IRI, as verified by serum tests, tissue staining, biomarker detection, and functional assessment. The protective effect of aC5a-FNA against cerebral IRI in living animals may pave the way for the translation of FNA from bench to bedside and broaden the horizon of FNA in the field of biomedicine.

Keywords

Framework nucleic acid; ischemic stroke; positron emission tomography; complement component 5a; intrathecal injection

[*]**Corresponding Authors**: djiang29@wisc.edu. Tel: (+1) 608-504-1696. wcai@uwhealth.org. Tel: (+1) 608-262-1749.

Supporting Information

The Supporting Information is available free of charge on the ACS Publications website at DOI: 10.1021/acs.nanolett.9b02958. Experimental section, characterizations of framework nucleic acids and its radiolabeling stability, as well as the biodistribution of FNAs in rats after intrathecal injection (PDF)

The authors declare no competing financial interest.

Strokes are the leading cause of disability globally, and the annual costs of strokes will rise 129% from 2010 to 2030.[1,2] Ischemic strokes account for ~80% of total cases of strokes. Cerebral ischemia-reperfusion injury (IRI) has been considered the main culprit and one of the primary obstacles in the treatment of ischemic strokes. Reperfusion injury following an ischemic stroke is a multifaceted process including oxidative stress, inflammation, and neuronal apoptosis and has been a major focus of neuroscience research. Excessive reactive oxygen species (ROS) generated from the cerebral IRI process can exhaust antioxidative defenses within the brain and lead to oxidative damage in the ischemic penumbra.[3] In addition to direct damages of brain tissues, ROS may also trigger the activation of the complement system that will rapidly magnify inflammatory responses.[4,5] The fifth component of complement (C5a), a pro-inflammatory polypeptide involved in complement activation, is a potent chemotactic factor that can recruit inflammatory cells, aggravate phagocytic activation, and enhance superoxide radical formation.[6,7] C5a has essential roles in exacerbating the vicious cycle of oxidative stress and inflammatory damage,[8] which increases the level of neuronal apoptosis and widens the infarct volume after cerebral IRI. A multitude of studies has demonstrated beneficial effects of utilizing antioxidant treatment[9] or C5a-blocking strategies[10] for brain IRI management. However, existing therapeutic strategies have shown limited efficacy[9] because single target treatment has often fallen short of dealing with complex mechanisms in time-sensitive cases such as cerebral IRI. Therefore, the development of multifunctional treatment has piqued great interest in the management of ischemic strokes.

Recent advances in nanomedicine have enabled innovative treatment of diseases using multifunctional nanomaterials.[11,12] However, nanoparticles are generally nonspecifically cleared by the mononuclear phagocyte system (e.g., the liver and spleen) or the urinary system. This substantially hampers the ability of nanomaterials to cross the blood–brain barrier (BBB) and limits their therapeutic applications for ischemic strokes. Intrathecal injection of nanomedicines directly introduces them into the cerebrospinal fluid (CSF), which improves their delivery to the brain and makes it possible to modify the brain microenvironment.[13] Here, a framework nucleic acid (FNA) was radiolabeled with ^{89}Zr, and its biodistribution in vivo was examined by using positron emission tomography (PET) imaging after intrathecal injection. However, evaluating biodistribution is not the final goal, and the development of specific therapy for cerebral IRI is an unmet clinical demand.

Framework nucleic acids, DNA frameworks built only by oligonucleotides, have recently garnered significant interest in biomedical applications due to some of their significant advantages such as low immunogenicity, excellent biocompatibility, and high delivery efficiencies.[14–17] Here, a bipyramidal FNA was used as a drug-loading platform for delivering anti-C5a aptamers (aC5a), a short single-stranded oligonucleotide with high affinity and specificity for C5a, to block the binding of C5a to CD88 (C5a receptor) and reduce C5a-mediated inflammatory and neuronal damage.[18] When delivered alone, this aC5a aptamer is susceptible to nuclease degradation and unstable in serum. Nanovesicles, such as FNA, may load aC5a with enhanced in vivo stability for targeted treatment. Recently, we demonstrated that FNAs in forms of DNA origami nanostructures could prevent acute kidney injury by scavenging ROS.[19]

Here, a bipyramidal FNA loaded with C5a aptamers (aC5a-FNA) was prepared.[20,21] We hypothesize that aC5a-FNA has integrated functions of scavenging free radicals and blocking C5a-mediated neurotoxicity to inhibit cerebral IRI. Utilizing intrathecal injection to attain a high accumulation of aC5a-FNA in the penumbra, we focus on the dynamics of this system to alleviate brain IRI in vivo (Figure 1). The detailed mechanism of IRI prevention using aC5a-FNA was investigated in depth, including the changes of ROS-related molecules and C5a, release of pro-inflammatory cytokines, recruitment of activated microglia and neutrophils, and the evaluation of damage volume and neurological function. This study provides novel perspectives for the development of FNA to address the unmet clinical need for ischemic stroke therapy.

Results and Discussion.

Multiantioxidative Activities of FNA.

Bipyramidal framework nucleic acids (FNAs) and aC5a-FNA were synthesized via a single-step annealing procedure reported previously (Figure 1 and Table S1).[22] Atomic force microscopy imaging and dynamic light scattering measurement showed that the morphology of the FNA and aC5a-FNA was uniform with an average diameter of approximately 10 nm (Figures S1 and S2). Six overhangs were designed on the edges of each FNA to enable subsequent functionalization with a deferoxamine-conjugated ssDNA for ^{89}Zr-labeling. The FNA and aC5a-FNA are highly hydrophilic and can be well-dispersed in water or PBS. The complementary single-stranded DNA could be efficiently radiolabeled with Zr-89 with a labeling efficiency of higher than 80% within 1 h of incubation (Figure S3). The 89Zr-labeled aC5a-FNA displayed a high radiolabeling stability in PBS and rat serum (Figure S4).

Since oxidative stress has a primary role in cerebral IRI, three representatives of ROS, including 2,2′-azino-bis(3-ethylbenzothiazoline-6-sulfonic acid) (ABTS), superoxide ($O_2^{\bullet-}$), and hydroxyl radical ($^{\bullet}OH$), were selected to investigate the ROS-scavenging activity of FNA. Both FNA and aC5a-FNA showed a high ROS eliminating property in a concentration-dependent manner when incubated with ABTS radicals (Figure 2A). Similarly, both assays with $O_2^{\bullet-}$ and $^{\bullet}OH$ radicals demonstrated high sensitivity and concentration-dependent scavenging of all of the FNA or aC5a-FNA (Figure 2B,C). However, there was no significant difference in the scavenging efficiency of either FNA or aC5a-FNA, suggesting that aC5a did not affect the antioxidative activity of aC5a-FNA. These results demonstrated that FNA and aC5a-FNA were robust multiantioxidant scavengers of ROS, which was in accordance with previous studies demonstrating that ROS may react with DNA via redox reactions.[23]

To investigate the protective role of aC5a-FNA on neurons against oxidative stress, we incubated H_2O_2 with primary neurons from SD rats and examined their capability of scavenging ROS on the cellular level. In comparison with the control cells, H_2O_2 treatment of primary neuron cells resulted in a significant increase of intracellular ROS on neurons, which later led to cell damage from oxidative stress. Following treatment with FNA or aC5a-FNA, lower levels of intracellular ROS concentrations were observed (Figure 2D,E). This data demonstrated that both FNA and aC5a-FNA have equally robust antioxidant activities and are concentration-dependent in solution and on the cellular level.

Receptor-Binding Assay and Functional Activity of FNA.

C5a, a protein fragment released from complement component C5, can bind the C5aR myeloid receptor with high affinity.[24] The binding of C5a to C5aR can rapidly augment inflammatory responses by recruiting inflammatory cells or by triggering the production and release of proinflammatory ROS.[25] To evaluate the efficiency of aC5a-FNA on blocking the binding of C5a/C5aR (Figure 2F), ^{89}Zr-labeled C5a bound to C5aR on polymorphonuclear neutrophils (PMNs) could be competed against by progressively increasing concentrations of aC5a or aC5a-FNA. The 50% inhibitory concentrations (IC50) were found to be 1.10 nmol/L (aC5a) and 1.49 nmol/L (aC5a-FNA). In the same assay using microglia (Figure 2G), the IC_{50} values were found to be 1.36 nmol/L (aC5a) and 1.82 nmol/L (aC5a-FNA). The minimal difference in IC_{50} between aC5a and aC5a-FNA suggested that both aC5a and aC5a-FNA had similar abilities to block C5a/C5aR binding on PMNs and microglia.

Complement component C5a, as one of the most potent inflammatory chemo-attractants, has been implicated in PMNs recruitment and microglial chemotaxis.[26] A previous study showed that the chemotaxis of inflammatory cells in response to C5a could be efficiently ablated by treatment with a PEGylated biostable C5a aptamer.[18] Here, to investigate whether aC5a-FNA could inhibit C5a-mediated chemotaxis, a cell migration assay was performed by using trans-wells (Figure 2H,I). Compared with the free C5a group, fewer PMNs and microglia were found in groups treated with aC5a or aC5a-FNA, suggesting that both aC5a and aC5a-FNA may reduce the C5a-mediated cell migration.

Biodistribution of FNA in the Brain Following Intrathecal Injection.

FNA can be easily radiolabeled via the hybridization of 89Zr-radiolabeled single-stranded oligonucleotides.[16,19,27] Thin-layer chromatography showed that both ^{89}Zr-FNA and ^{89}Zr-aC5a-FNA were stable in PBS and rat serum, where more than 60% of ^{89}Zr-FNA and ^{89}Zr-aC5a-FNA remained intact within 24 h, where the framework, size, and behavior of ^{89}Zr-FNA and ^{89}Zr-aC5a-FNA remained consistent.

Due to the BBB,[28] very few small-molecule drugs can be delivered to the brain by systemic administration. To overcome this limitation, intrathecal administration was performed to directly deliver therapeutic agents into the cerebral penumbra, which is particularly desired for maximizing local drug concentrations. The experimental time schedule for inducing rat IRI is shown in Figure 3A. Magnetic resonance imaging (MRI) revealed that the cerebral IRI model was successfully established due to the presence of significant ischemic brain damage (yellow circles) in the PBS-treated group (Figure 3B). To investigate the biodistribution of ^{89}Zr-labeled FNA, PET imaging was performed at 15 min, and 3 and 9 h after ^{89}Zr-FNAs were administered intrathecally into rats with IRI. Axial, coronal, and sagittal PET images clearly showed that 89Zr-FNA highly accumulated within the cerebrospinal fluid and brain at 15 min postinjection (p.i.). At later time points, 89Zr-FNA uptake in the brain slowly decreased and almost disappeared at 9 h p.i. (Figure 3C–E). Quantification of 89Zr-aC5a-FNA in the brain, heart, lung, liver, kidneys, and spleen was also performed (Figures S5–S7) based on region-of-interest analysis of different organs ex vivo (Figure S8). ^{89}Zr-FNA was later found in the blood pool, which is due to its transportation from the brain to the heart via the superior sagittal sinus. This is the first time that PET imaging has been used to

dynamically and noninvasively investigate the distribution of FNA in the central nervous system after intrathecal injection.

To further investigate the distribution of aC5a-FNA within the brain, rats administered 89Zr-FNA intrathecally were euthanized and their brains were resected 3 h after IRI and scanned using PET imaging. As shown in Figure 4A,B, no obvious differences were found between ^{89}Zr-FNA and ^{89}ZraC5a-FNA after intrathecal injection, suggesting that hybridization with aC5a did not change the distribution of FNA. Additionally, no differences were found between the left and right sides of the brain. Axial, coronal, and sagittal PET images of ^{89}Zr-FNA showed that they accumulated in the ventricles, the cisterns, and the subarachnoid space (Figure 4C). The biodistribution of ^{89}Zr-FNA was consistent with the route of CSF circulation: 89Zr-FNA followed the CSF through the ventricles, cisterns, and subarachnoid space and was finally absorbed into the blood at the arachnoid villi. This data demonstrated that DNA frameworks rapidly perfuse into the CSF and spread out within the brain after intrathecal injection, which is a necessary requirement for their potential protection of cerebral IRI.

Intrathecal administration introduces the therapeutics into the CSF in the subarachnoid space, which is an effective strategy to bypass the blood–brain barrier. The intrathecal route is an ideal route of administration for certain therapeutic drugs with good biocompatibility and low neurotoxicity for cerebral IRI. However, limitations also exist, such as the technical difficulty of performing the procedure and increased possibilities of infection in the central nervous system.

Antioxidative Activities of aC5a-FNA in Vivo.

Substantial evidence has confirmed that an ischemic stroke triggers complement system activation, which results in an increase of anaphylatoxin C5a in the plasma and ischemic penumbra and triggers the inflammatory cascade.[29] Therefore, we investigated the therapeutic effects of aC5a-FNA on C5a expression, oxidative stress, and inflammation in penumbra (Figure 5A). Higher concentrations of C5a were found in the plasma and penumbra in PBS-treated IRI rats compared to those in the sham group (Figure 5B,C). Compared with the PBS-treated group, decreased levels of C5a were found after FNA treatment. This data suggested that the increase of C5a after cerebral IRI could be attenuated with treatment using aC5a-FNA.

FNAs were recently found to possess an intrinsic ability to scavenge detrimental ROS and alleviate acute injury of the kidneys.[19] To investigate the level of oxidative stress in the context of cerebral IRI, superoxide dismutase (SOD) and malondialdehyde (MDA) levels were measured in the brain homogenates of each treatment group.[30] Rats were euthanized 3 days after cerebral IRI; the brains of each group were collected and homogenated. Compared to the PBS-treated group, significantly increased levels of SOD and decreased levels of MDA were found in both the FNA and aC5a-FNA treatment groups. This suggested that FNA alone and aC5a-FNA effectively inhibited oxidative stress in penumbra (Figure 5D,E). However, there is no significant difference in both FNA and aC5a-FNA groups, indicating that FNA and aC5a-FNA have a comparable efficacy regarding ROS

neutralization due to their similar antioxidative capacities established by our in vitro experiments.

Anti-Inflammatory Effect of aC5a-FNA in Vivo.

C5a, as a potent neurotoxin, is responsible for recruiting PMNs and/or activated microglia into the penumbra by binding with C5aR, which plays a vital role in deteriorating neuronal damage during and after cerebra IRI.[31,32] To investigate whether aC5a-FNA could inhibit C5a-mediated chemotaxis of inflammatory cells, activation of microglia ($CD68^+$/$Iba\text{-}1^+$ cells) and inflammatory cells ($CD11b^+$ cells) in the penumbra was investigated using confocal microscopy. Compared to the PBS-treated group, significantly fewer $CD68^+$/$Iba\text{-}1^+$ and $CD11b^+$ inflammatory cells were identified in the aC5a-FNA treatment group at 3 days after cerebral IRI (Figure 5F,G). The quantitative analysis further confirmed that aC5a-FNA treatment resulted in a significant decrease of microglial activation and the infiltration of $CD11b^+$ inflammatory cells into the penumbra (Figure 5H,I). In comparison, both studies showed that FNA alone was unable to inhibit the activation of $CD68^+$/$Iba\text{-}1^+$ and $CD11b^+$ inflammatory cells. This data demonstrated that aC5a-FNA could efficiently block C5a-stimulated microglial activation and chemotaxis of peripheral blood inflammatory cells.

To investigate whether aC5a-FNA treatment could reduce the release of pro-inflammatory factors, the expression of IL-6 and TNF-α in the penumbra was measured using ELISA assays. Compared with the PBS-treated group, significantly lower levels of IL-1β and TNF-α were observed in FNA or aC5a-FNA treatment groups. Notably, the levels of IL-1β and TNF-α expression in the aC5a-FNA group were lower than those in the FNA group (Figure 5G–K), indicating that aC5a has an essential anti-inflammatory role after incorporated with FNA, which could effectively reduce inflammation after IRI and improve treatment efficacy.

aC5a-FNA Is Cerebral-Protective for Rats with Brain IRI.

To determine whether the treatment of aC5a-FNA could protect neurons against oxidative stress, immunofluorescent staining of Nissl (neurons), and cleaved Caspase-3 (apoptosis) was performed at 3 days after cerebral IRI (Figure 6A). The number of cleaved caspase-3 positive neurons was 229.3 ± 22.6/mm^2 in the PBS-treated group, 219.3 ± 19.6/mm^2 in the free aC5a group, 141.3 ± 14.7/mm^2 in the FNA group, and 93.4 ± 9.3/mm^2 in the aC5a-FNA group ($P < 0.01$), Thus, fewer cleaved caspase-3 positive cells were observed in the aC5a-FNA treatment group compared with other treatment groups because both aC5a and FNA contributed to the protection of neurons after cerebral IRI. Furthermore, the reverse transcription-polymerase chain reaction (RT-PCR) and real-time PCR confirmed decreased expression of caspase-3 in the aC5a-FNA treatment group than other groups (Figure 6B,C). This data showed that the treatment of aC5a-FNA could effectively protect neuronal apoptosis from IRI.

Triphenyl tetrazolium chloride (TTC) staining, an effective method to differentiate metabolically active and inactive tissues in the brain, has been widely used to evaluate the infarct size and volume after an ischemic stroke.[33] Our data showed that the infarct volumes in the PBS, aC5a, FNA, and aC5a-FNA groups were 41.6 ± 7.1, 40.2 ± 5.3, 28.2 ± 7.6, and 17.0 ± 5.6%, respectively (Figure 6D,E). MRI imaging was also performed to validate the

treatment efficacy, as shown in Figure S9. Compared with PBS-treated rats, no significant decrease in infarcted volume was found in the aC5a treatment group, suggesting its ineffectiveness for stroke treatment, probably because it is unstable in vivo. However, a significant decrease in the infarcted volume was found for both the FNA and aC5a-FNA treatment groups at 3 days after IRI compared to the PBS-treated group (Figure 6F). Importantly, rats in the aC5a-FNA treatment group had a smaller infarcted volume than rats in the FNA treatment group, indicating that aC5a-FNA is more effective in preventing IRI damage in animals.

Encouraged by the treatment results, the modified Neurological Severity Score (mNSS), including motor, sensory, and reflex tests, was further used to evaluate the neurological functions of all rats.[34] A higher score indicates severer damage. To test whether aC5a-FNA treatment can improve neurological functions, behavioral tests were performed at 1, 2, and 3 days after IRI. As shown in Figure 6G, severe behavioral deficits were found in the PBS and aC5a group, suggesting that both PBS and the unstable aC5a had no therapeutic effects on IRI rats. Compared with other groups, the lowest mNSS scores were found in the aC5a-FNA group, suggesting the optimal protective role of aC5a-FNA on improving brain functions of rats after cerebral IRI. Despite the positive protection induced by FNAs, scrutiny is necessary when delivering FNAs to the brain via intrathecal injection. In this study, at a dose of 0.05 mg/kg for rats with IRI, no sign of abnormality of any kind was observed. However, systematic evaluation of toxicity and dose optimization will be needed for clinical translation.

Conclusions.

In this study, we established a bipyramidal FNA as a multifunctional platform for cerebral IRI management. The DNA framework proved a potent antioxidant for three different types of ROS in solutions and on the cellular level to protect primary neurons from oxidative stress. The aC5a-loaded FNA may strongly bind to C5a and inhibit the chemotaxis of inflammatory cells in its response. To maximize the retention of aC5a-FNA in the brain of IRI rats, we performed intrathecal injection and used PET imaging to investigate and quantify its distribution. Results showed that aC5a-FNA may spread out in the ischemic penumbra. MRI imaging, TTC staining, and rat behavior scores further confirmed the protective role of aC5a-FNA for rat cerebral IRI.

Supplementary Material

Refer to Web version on PubMed Central for supplementary material.

ACKNOWLEDGMENTS

This work was supported, in part, by the University of Wisconsin-Madison and the National Institutes of Health (P30CA014520), National Natural Science Foundation of China (81760417, 81660230, and 81871031), and Science and Technology Program of Jiangxi, China (2016ACB21019 and 2018ACB20020).

REFERENCES

(1). Granger DN; Kvietys PR Reperfusion injury and reactive oxygen species: The evolution of a concept. Redox Biol. 2015, 6, 524–551. [PubMed: 26484802]

(2). Wang JY; Shen J; Gao Q; Ye ZG; Yang SY; Liang HW; Bruce IC; Luo BY; Xia Q Ischemic postconditioning protects against global cerebral ischemia/reperfusion-induced injury in rats. Stroke 2008, 39 (3), 983–90. [PubMed: 18239163]

(3). Kalogeris T; Bao Y; Korthuis RJ Mitochondrial reactive oxygen species: a double edged sword in ischemia/reperfusion vs preconditioning. Redox Biol. 2014, 2, 702–14. [PubMed: 24944913]

(4). Vogt W; Hesse D Activation of the fifth component of human complement by oxygen-derived free radicals, and by methionine oxidizing agents: a comparison. Immunobiology 1992, 184 (4–5), 384–91. [PubMed: 1592429]

(5). Collard CD; Agah A; Stahl GL Complement activation following reoxygenation of hypoxic human endothelial cells: role of intracellular reactive oxygen species, NF-kappaB and new protein synthesis. Immunopharmacology 1998, 39 (1), 39–50. [PubMed: 9667422]

(6). Activity Brain. Nat. Nanotechnol 2014, 9 (2) 85. [PubMed: 24496271]

(7). Monk PN; Scola AM; Madala P; Fairlie DP Function, structure and therapeutic potential of complement C5a receptors. Br. J. Pharmacol 2007, 152 (4), 429–48. [PubMed: 17603557]

(8). Ricklin D; Hajishengallis G; Yang K; Lambris JD Complement: a key system for immune surveillance and homeostasis. Nat. Immunol 2010, 11 (9), 785–97. [PubMed: 20720586]

(9). Margaill I; Plotkine M; Lerouet D Antioxidant strategies in the treatment of stroke. Free Radical Biol. Med 2005, 39 (4), 429–43. [PubMed: 16043015]

(10). Mizuma A; Yenari MA Anti-Inflammatory Targets for the Treatment of Reperfusion Injury in Stroke. Front Neurol 2017, 8, 467. [PubMed: 28936196]

(11). Rosenblum D; Joshi N; Tao W; Karp JM; Peer D Progress and challenges towards targeted delivery of cancer therapeutics. Nat. Commun 2018, 9 (1), 1410. [PubMed: 29650952]

(12). Lam FC; Morton SW; Wyckoff J; Vu Han TL; Hwang MK; Maffa A; Balkanska-Sinclair E; Yaffe MB; Floyd SR; Hammond PT Enhanced efficacy of combined Temozolomide and bromodomain inhibitor therapy for gliomas using targeted nanoparticles. Nat. Commun 2018, 9 (1), 1991. [PubMed: 29777137]

(13). Oliveira JM; Carvalho L; Silva-Correia J; Vieira S; Majchrzak M; Lukomska B; Stanaszek L; Strymecka P; Malysz-Cymborska I; Golubczyk D; Kalkowski L; Reis RL; Janowski M; Walczak P Hydrogel-based scaffolds to support intrathecal stem cell transplantation as a gateway to the spinal cord: clinical needs, biomaterials, and imaging technologies. NPJ. Regen Med 2018, 3, 8. [PubMed: 29644098]

(14). Jiang Q; Song C; Nangreave J; Liu X; Lin L; Qiu D; Wang ZG; Zou G; Liang X; Yan H; Ding B DNA origami as a carrier for circumvention of drug resistance. J. Am. Chem. Soc 2012, 134 (32), 13396–403. [PubMed: 22803823]

(15). Zhang F; Jiang S; Wu S; Li Y; Mao C; Liu Y; Yan H Complex wireframe DNA origami nanostructures with multi-arm junction vertices. Nat. Nanotechnol 2015, 10 (9), 779–84. [PubMed: 26192207]

(16). Jiang D; Sun Y; Li J; Li Q; Lv M; Zhu B; Tian T; Cheng D; Xia J; Zhang L; Wang L; Huang Q; Shi J; Fan C Multiple-Armed Tetrahedral DNA Nanostructures for Tumor-Targeting, Dual-Modality in Vivo Imaging. ACS Appl. Mater. Interfaces 2016, 8 (7), 4378–84. [PubMed: 26878704]

(17). Ge Z; Gu H; Li Q; Fan C Concept and Development of Framework Nucleic Acids. J. Am. Chem. Soc 2018, 140 (51), 17808–17819. [PubMed: 30516961]

(18). Yatime L; Maasch C; Hoehlig K; Klussmann S; Andersen GR; Vater A Structural basis for the targeting of complement anaphylatoxin C5a using a mixed L-RNA/L-DNA aptamer. Nat. Commun 2015, 6, 6481. [PubMed: 25901944]

(19). Jiang D; Ge Z; Im HJ; England CG; Ni D; Hou J; Zhang L; Kutyreff CJ; Yan Y; Liu Y; Cho SY; Engle JW; Shi J; Huang P; Fan C; Yan H; Cai W DNA origami nanostructures can exhibit preferential renal uptake and alleviate acute kidney injury. Nat. Biomed Eng 2018, 2 (11), 865–877. [PubMed: 30505626]

(20). Erben CM; Goodman RP; Turberfield AJ A self-assembled DNA bipyramid. J. Am. Chem. Soc 2007, 129 (22), 6992–3. [PubMed: 17500526]

(21). Li J; Jiang D; Bao B; He Y; Liu L; Wang X Radiolabeling of DNA Bipyramid and Preliminary Biological Evaluation in Mice. Bioconjugate Chem. 2016, 27 (4), 905–10.

(22). Rothemund PW Folding DNA to create nanoscale shapes and patterns. Nature 2006, 440 (7082), 297–302. [PubMed: 16541064]

(23). Hemnani T; Parihar MS Reactive oxygen species and oxidative DNA damage. Indian J. Physiol Pharmacol 1998, 42 (4), 440–52. [PubMed: 10874342]

(24). Merle NS; Noe R; Halbwachs-Mecarelli L; Fremeaux-Bacchi V; Roumenina LT Complement System Part II: Role in Immunity. Front. Immunol 2015, 6, 257. [PubMed: 26074922]

(25). Patel SN; Berghout J; Lovegrove FE; Ayi K; Conroy A; Serghides L; Min-oo G; Gowda DC; Sarma JV; Rittirsch D; Ward PA; Liles WC; Gros P; Kain KC C5 deficiency and C5a or C5aR blockade protects against cerebral malaria. J. Exp. Med 2008, 205 (5), 1133–43. [PubMed: 18426986]

(26). Pavlovski D; Thundyil J; Monk PN; Wetsel RA; Taylor SM; Woodruff TM Generation of complement component C5a by ischemic neurons promotes neuronal apoptosis. FASEB J. 2012, 26 (9), 3680–90. [PubMed: 22651932]

(27). Jiang D; Im H-J; Boleyn ME; England CG; Ni D; Kang L; Engle JW; Huang P; Lan X; Cai W Efficient renal clearance of DNA tetrahedron nanoparticles enables quantitative evaluation of kidney function. Nano Res. 2019, 12 (3), 637–642.

(28). Shi Y; Zhang L; Pu H; Mao L; Hu X; Jiang X; Xu N; Stetler RA; Zhang F; Liu X; Leak RK; Keep RF; Ji X; Chen J Rapid endothelial cytoskeletal reorganization enables early blood-brain barrier disruption and long-term ischaemic reperfusion brain injury. Nat. Commun 2016, 7, 10523. [PubMed: 26813496]

(29). Kim GH; Mocco J; Hahn DK; Kellner CP; Komotar RJ; Ducruet AF; Mack WJ; Connolly ES Jr. Protective effect of C5a receptor inhibition after murine reperfused stroke. Neurosurgery 2008, 63 (1), 122. [PubMed: 18728577]

(30). Kuyumcu F; Aycan A Evaluation of Oxidative Stress Levels and Antioxidant Enzyme Activities in Burst Fractures. Med. Sci. Monit 2018, 24, 225–234. [PubMed: 29324724]

(31). Kalogeris T; Baines CP; Krenz M; Korthuis RJ Cell biology of ischemia/reperfusion injury. Int. RevCell Mol. Biol 2012, 298, 229–317.

(32). Gorsuch WB; Chrysanthou E; Schwaeble WJ; Stahl GL The complement system in ischemia-reperfusion injuries. Immunobiology 2012, 217 (11), 1026–33. [PubMed: 22964228]

(33). Wang Y; Li SY; Shen S; Wang J Protecting neurons from cerebral ischemia/reperfusion injury via nanoparticle-mediated delivery of an siRNA to inhibit microglial neurotoxicity. Biomaterials 2018, 161, 95–105. [PubMed: 29421566]

(34). Wang Y; Luo J; Li SY Nano-Curcumin Simultaneously Protects the Blood-Brain Barrier and Reduces M1Microglial Activation During Cerebral Ischemia-Reperfusion Injury. ACS Appl. Mater. Interfaces 2019, 11 (4), 3763–3770. [PubMed: 30618231]

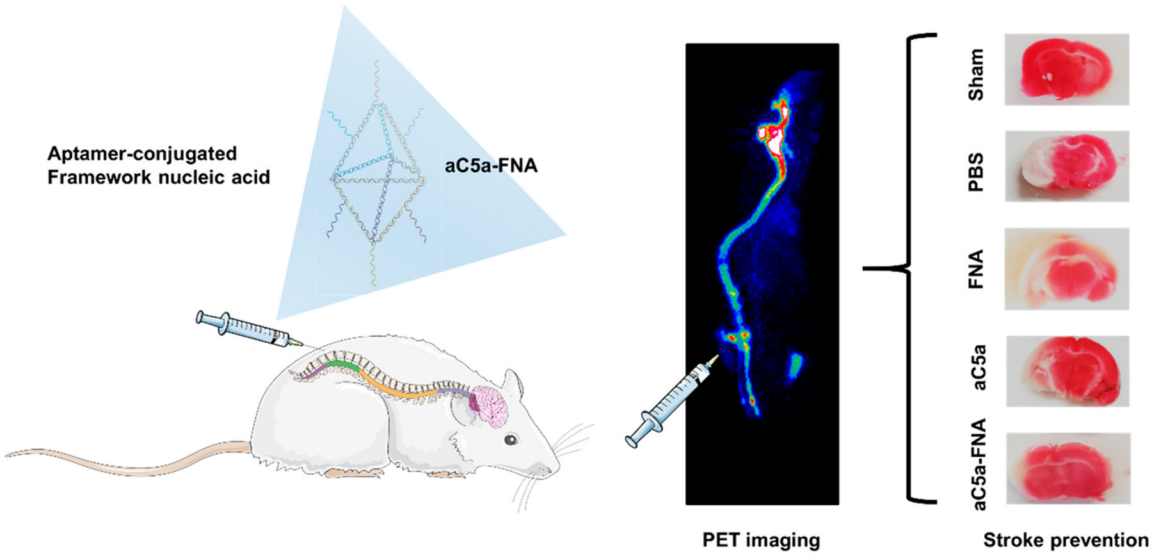

Figure 1.

Schematic of cerebral ischemia-reperfusion injury (IRI) treatment using an anticomplement component 5a (aC5a) loaded framework nucleic acid (aC5a-FNA) after intrathecal injection. PET imaging and brain tissue staining confirmed the biodistribution and treatment efficacy of FNA for brain IRI management.

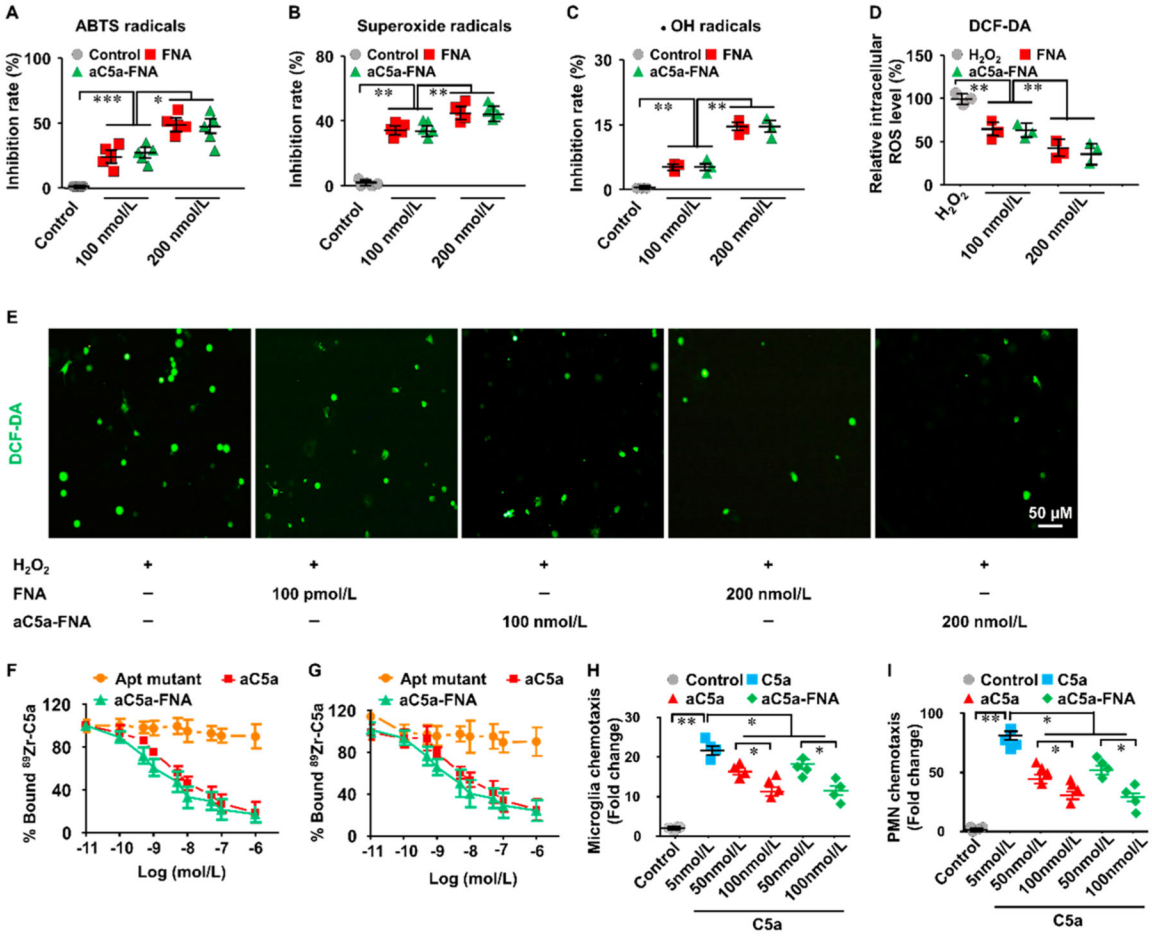

Figure 2.

Multiantioxidative roles of the aC5a-FNA on neurons. Inhibition rate of aC5a-FNA on (A) ABTS radicals, (B) superoxide radicals, and (C) •OH radicals. (D) ROS levels in untreated and FNA-treated neurons incubated with 0.2 mM H_2O_2 ($n = 3$, mean ± SD, $^*P < 0.05$, $^{**}P < 0.01$, $^{***}P < 0.001$). (E) Representative ROS staining of neurons incubated with H_2O_2 treated with different concentrations of FNA. Scale bar: 50 μm. (F) Cell binding assay of aC5a and aC5a-FNA using polymorphonuclear neutrophils (PMNs) ($n = 3$, Mean ± SD). (G) Cell binding assay of aC5a and aC5a-FNA using microglia ($n = 3$, mean ± SD). (H) C5a-activated chemotaxis of PMNs can be inhibited by using free aC5a or aC5a-FNA (n=4, mean ± SD, $^*P$< 0.05, $^{**}P$< 0.01). (I) C5a-activated chemotaxis of microglia can be inhibited either free aC5a or aC5a-FNA (n= 4, mean ± SD, $^*P$< 0.05, $^{**}P$< 0.01).

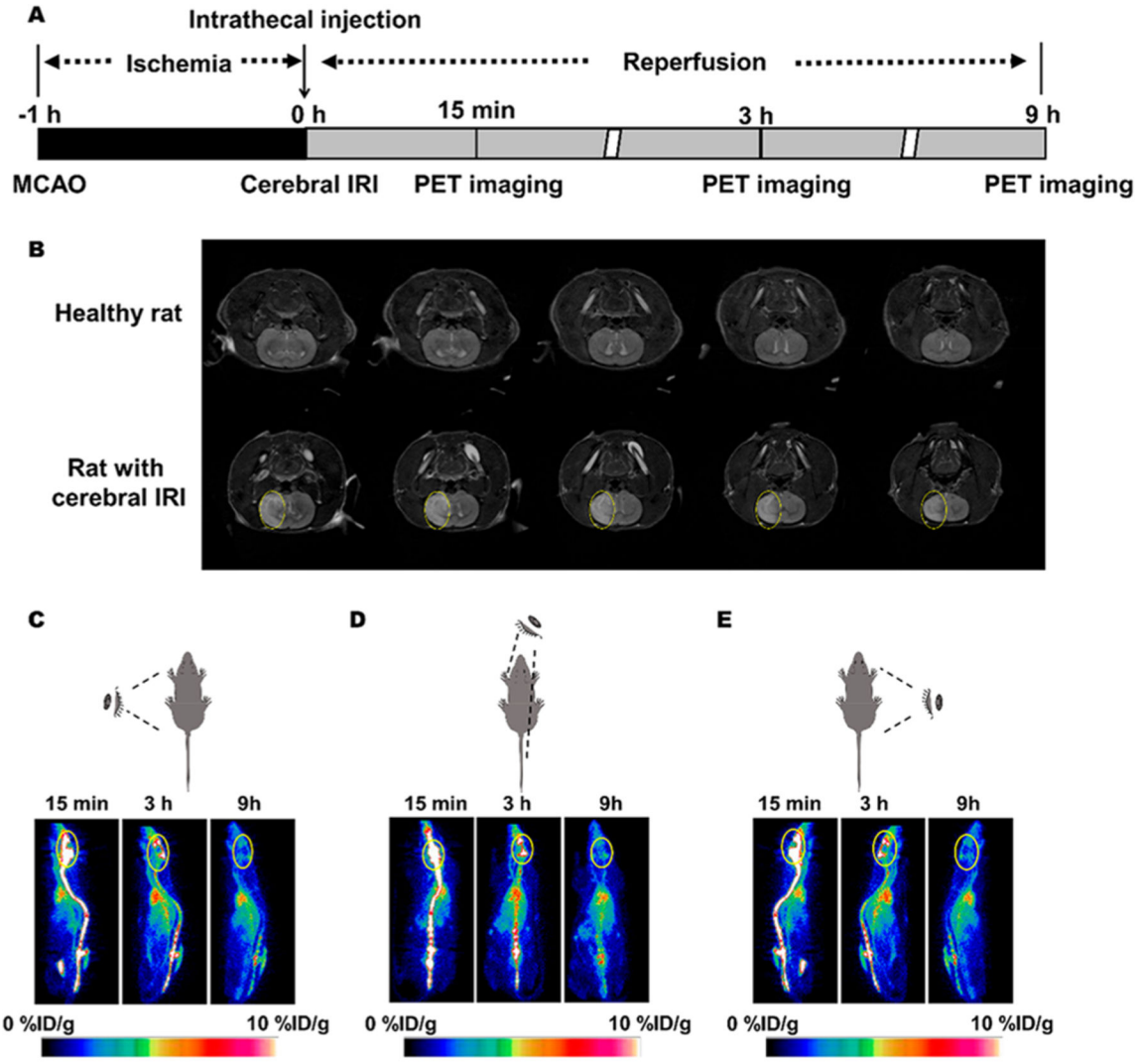

Figure 3.

PET imaging of aC5a-FNA in rats with cerebral IRI. (A) Time schedule of cerebral IRI model establishment, treatment, and PET imaging using aC5a-FNA. (B)T2-weighted magnetic resonance image of rats at 3 days after IRI. The white area represents the lesion (marked by yellow circle). Representative longitudinal PET images of ^{89}Zr-labeled aC5a-FNA from (C) the left, (D) top, and (E) right view. Yellow circles denote the brain.

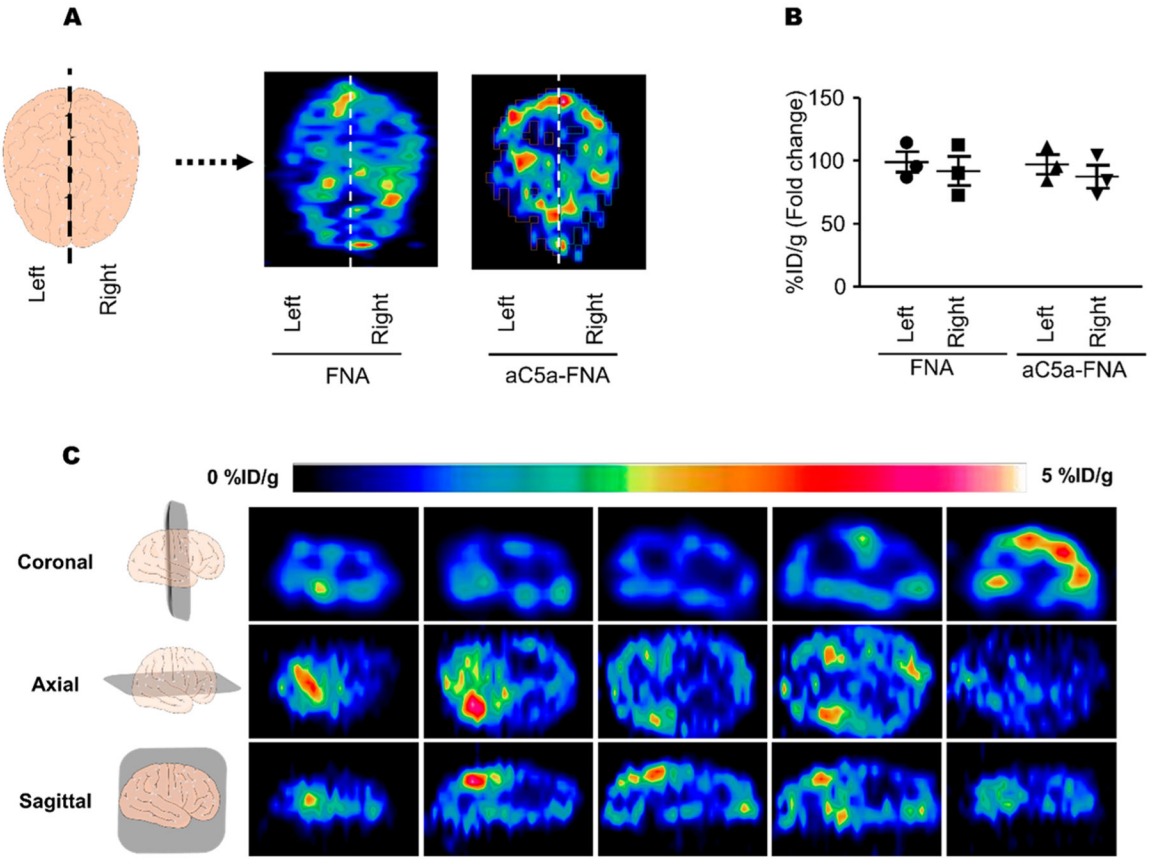

Figure 4.

The biodistribution of FNA in the brains of rats with cerebral IRI. (A) Representative PET images of both the FNA and aC5a-FNA in the brain at 3 h after IRI. (B) Quantitative analysis of FNA in the left and right side of the brain. Data represent mean ± SD from three independent replicates. (C) Representative sections of PET images of ^{89}Zr-labeled aC5a-FNA were shown at 3 h after cerebral IRI.

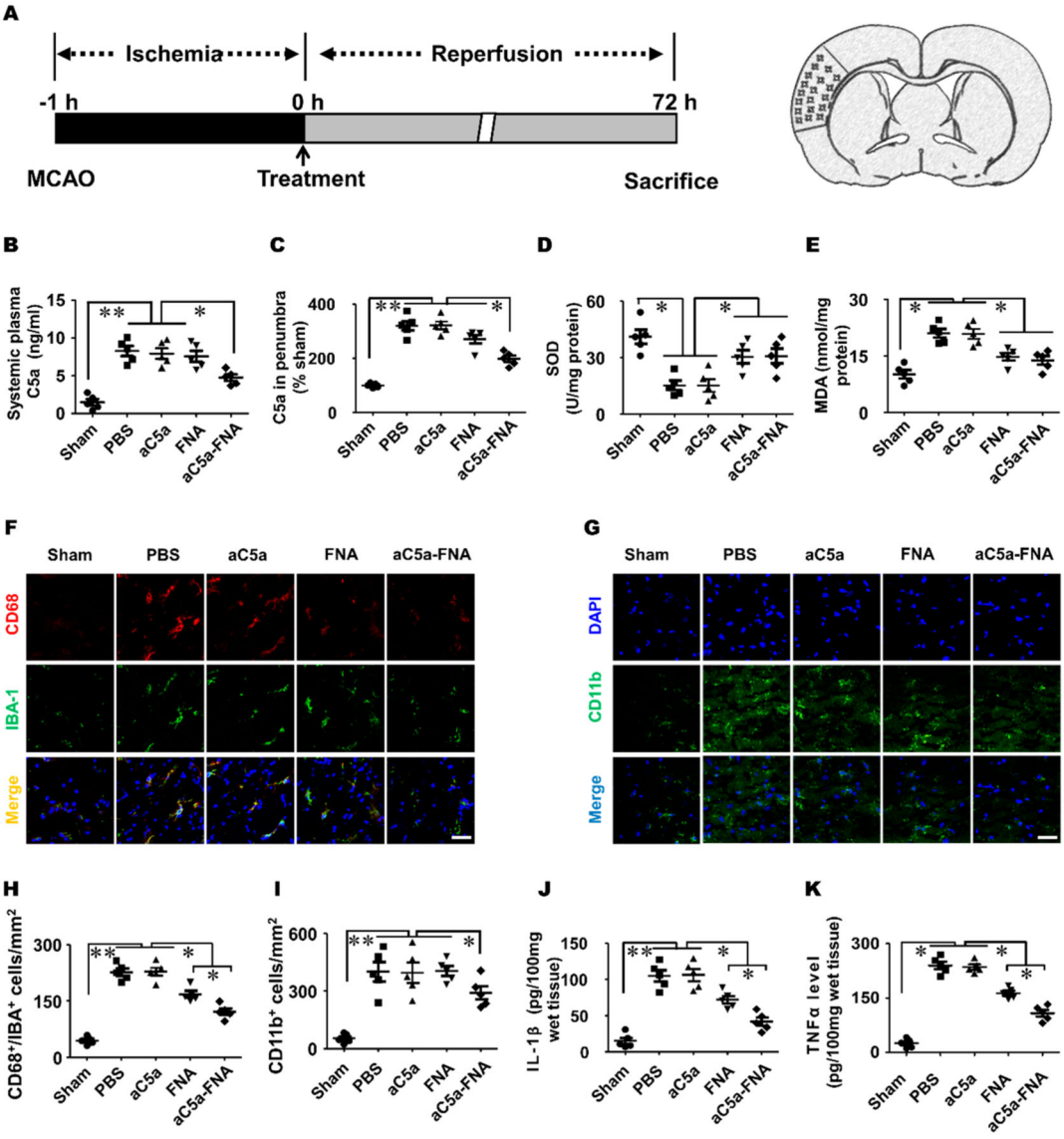

Figure 5.

The aC5a-FNA treatment inhibited oxidative stress and inflammatory in brain penumbra. (A) Time schedule for cerebral IRI establishment and analysis in the ischemic cortex. The change of C5a in (B) the plasma and (C) penumbra. The level of (D) SOD and (E) MDA in the ischemic penumbra (mean ± SD, $n = 5$, ** $P < 0.01$). Immunofluorescent staining of (F) $CD68^+/Iba\text{-}1^+$ and (G) CD11b+ inflammatory cells at 3 days after cerebral IRI. Scale bar: 25 μm. Quantitative analysis of (H) CD68 and Iba-1 double-positive cells and (I) $CD11b^+$ inflammatory cells in the penumbra and (J) IL-1β levels and (K) TNF-α levels in the ischemic penumbra were determined by ELISA assays (mean ± SD, $n = 5$, ** $P < 0.01$).

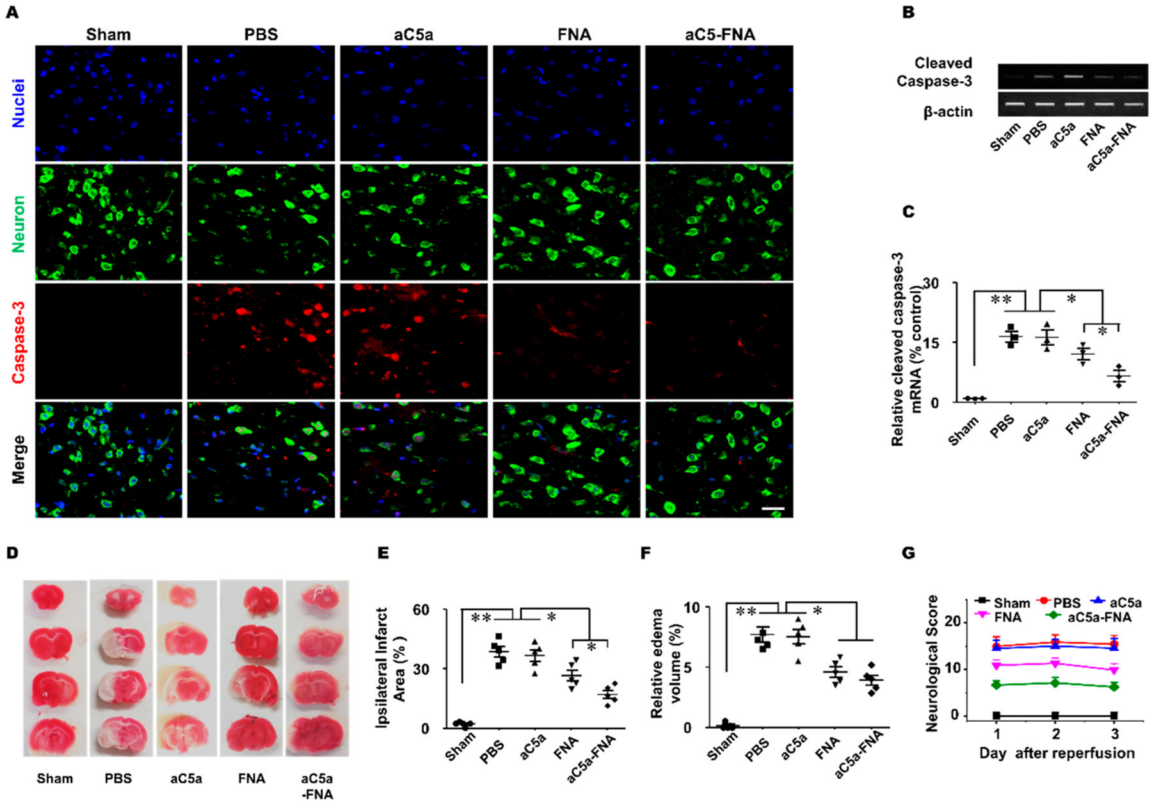

Figure 6.

The aC5a-FNA treatment attenuates brain IRI. (A) Activated caspase-3 (red) and Nissl staining (green) were detected by confocal microscopy in the ipsilateral cortex (scale bar, 25 μm). Activated caspase-3 gene expression in the ischemic penumbra was detected using (B) gel electrophoresis and (C) real-time PCR (mean ± SD, $n = 3$, ** $P < 0.01$). (D) Representative TTC staining, quantitative analysis of (E) edema volume, (F) infarct volume, and (G) neurological scores in different groups ($n > 3$, mean ± SD, *$P < 0.05$, **$P < 0.01$).